Query Details

Back to Main Page

1. In the sentence beginning 'This scenario is...', please define '<Emphasis Type="Italic">T</Emphasis>_c'.

2. Please check your article carefully, coordinate with any co-authors and enter all final edits clearly in the eproof, remembering to save frequently. Once corrections are submitted, we cannot routinely make further changes to the article.

3. Note that the eproof should be amended in only one browser window at any one time; otherwise changes will be overwritten.

4. Author surnames have been highlighted. Please check these carefully and adjust if the first name or surname is marked up incorrectly, as this will affect indexing of your article in public repositories such as PubMed. Also, carefully check the spelling and numbering of all author names and affiliations, and the corresponding author(s) email address(es). Please note that email addresses should only be included for designated corresponding authors, and you cannot change corresponding authors at this stage except to correct errors made during typesetting.

5. You cannot alter accepted Supplementary Information files except for critical changes to scientific content. If you do resupply any files, please also provide a brief (but complete) list of changes. If these are not considered scientific changes, any altered Supplementary files will not be used, only the originally accepted version will be published.

6. Please check Figures for accuracy as they have been relabelled. Please markup minor changes in the eProof. For major changes, please provide revised figures. (Please note that in the eProof the figure resolution will appear at lower resolution than in the pdf and html versions of your paper.)

7. If applicable, please ensure that any accession codes and datasets whose DOIs or other identifiers are mentioned in the paper are scheduled for public release as soon as possible, we recommend within a few days of submitting your proof, and update the database record with publication details from this article once available.

8. In the sentence beginning 'Sr2IrO4 is isostructural...', please define '<Emphasis Type="Italic">J</Emphasis>_{eff}'.

9. Please check use of bold and italic font throughout maths. We conform to the style that vectors are set in bold roman font. The magnitude of a vector is set in non-bold italics, as are scalar components, tensors and matrices. Units are in roman. Subscripts and superscripts are upright unless they represent variables. Please ensure your text is consistent with this throughout.

10. Variables are set in italics for style, and sub/superscripts non-italic unless they represent variables. Please check that all symbols are formatted correctly.

11. Please confirm the y axis label on fig 1d is correct.

12. There is no grey shaded area in Fig. 2b. Please clarify.

13. There are no open symbols at <Emphasis Type="Italic">T</Emphasis> = 0 in Fig. 2b. Please clarify.

14. In the expression in the caption for Fig. 4b, it was assumed that the d’s represent differentials and so were rendered upright. Please correct if wrong. Also note that the final closing parenthesis is unmatched. Please correct.

15. Please note, we reserve ‘significant’ and its derivatives for statistical significance. Please reword if this is not the intended meaning (for example to important, notable, substantial).

16. Please confirm rewording of the phrase: "using a scanning electron microscope (JSM-6610LV, JEOL) and an energy-dispersive X-ray spectroscope (Oxford Instruments)".

17. Please define PPMS in the Acknowledgements.

18. We have noticed that figures citation in main text are not in sequence order. Please check and suggest.

19. If ref. 34 (preprint) has now been published in final peer-reviewed form, please update the reference details if appropriate.

Article

Carrier density crossover and quasiparticle mass enhancement in a doped 5∂ Mott insulator

Yu-Te Hsu✉
Email : ythsu@phys.nthu.edu.tw
Affiliationids : Aff1 Aff2, Correspondingaffiliationid : Aff1

Andreas Rydh Affiliationids : Aff3

Maarten Berben Affiliationids : Aff1

Caitlin Duffy Affiliationids : Aff1

Alberto de la Torre Affiliationids : Aff4

Robin S. Perry Affiliationids : Aff5 Aff6

Nigel E. Hussey✉
Email : n.e.hussey@bristol.ac.uk
Affiliationids : Aff1 Aff7, Correspondingaffiliationid : Aff1

Aff1 High Field Magnet Laboratory (HFML-FELIX) and Institute for Molecules and Materials, Radboud University, Nijmegen, The Netherlands

Aff2 Department of Physics, National Tsing Hua University, Hsinchu, Taiwan

Aff3 Department of Physics, Stockholm University, Stockholm, Sweden

Aff4 Department of Physics, Northeastern University, Boston, MA, USA

Aff5 London Centre for Nanotechnology and Dept. of Physics and Astronomy, University College London, London, UK

Aff6 ISIS Neutron and Muon Source, Rutherford Appleton Laboratory, Harwell, UK

Aff7 H. H. Wills Physics Laboratory, University of Bristol, Bristol, UK

Received: 25 July 2023 / Accepted: 23 May 2024

Abstract

High-temperature superconductivity in cuprates emerges upon doping the parent Mott insulator. Key features of the low-doped cuprate superconductors include an effective carrier density that tracks the number of doped holes, the emergence of an anisotropic pseudogap that is characterized by disconnected Fermi arcs and the closure of the gap at a critical doping level. In Sr_2IrO_4, a spin–orbit-coupled Mott insulator often regarded as a 5*d* analogue of the cuprates, surface probes have also revealed the emergence of an anisotropic pseudogap and Fermi arcs under electron doping. However, neither the corresponding critical doping nor the bulk signatures of pseudogap closure have yet been observed. Here we demonstrate that electron-doped Sr_2IrO_4 exhibits a critical doping level with a marked crossover in the effective carrier density at low temperatures. This is accompanied by a five-orders-of-magnitude increase in conductivity and a sixfold enhancement in the electronic specific heat. These collective findings resemble the bulk pseudogap phenomenology in cuprates. However, given that electron-doped Sr_2IrO_4 is non-superconducting, it suggests that the pseudogap may not be a state of precursor pairing. Therefore, our results narrow the search for the key ingredient underpinning the formation of the superconducting condensate in doped Mott insulators.

Editor's Summary

The pseudogap in cuprates is often linked to superconductivity. Now bulk evidence for a pseudogap is found in doped non-superconducting Sr_2IrO_4, revealing that pseudogaps in doped Mott insulators are not necessarily a precursor to superconductivity.

Main

There are two principal pathways along which a system of itinerant electrons approaches a Mott state[1]. When the interactions are predominantly local, a paramagnetic Fermi liquid survives up until the metal–insulator transition, albeit with a divergent quasiparticle mass. This type of transition is observed, for instance, in Sr-doped $LaTiO_3$ (ref. [2]). The alternative transition to the Mott state is characterized by a vanishing carrier number and a non-diverging quasiparticle mass. This scenario is believed to be realized in the high-T_c **AQ1** cuprates[3, 4], although the oxygen 2*p* states render the system a charge-transfer insulator. Moreover, the electronic states in cuprates are *k*-space differentiated such that mobile carriers are found only near the zone diagonals, due to the presence of an anisotropic pseudogap (PG) that removes low-energy spectral weight preferentially near the zone edges and breaks the underlying Fermi surface into a series of disconnected ‘Fermi arcs’[5]. **AQ2** **AQ3** **AQ4** **AQ5** **AQ6** **AQ7**

Since its discovery[6], the precise phase extent and phenomenology of the PG have been a subject of intense scrutiny and debate, although a consensus is beginning to emerge, that of an anisotropic, states-non-conserving gap whose amplitude diminishes linearly with hole doping (*p*) and collapses at a critical doping *p** deep within the superconducting phase boundary[7, 8]. Understanding the origin of PG formation is widely regarded as a key step in the elucidation, not only of the Mott transition in cuprates, but also of the pairing mechanism for high-T_c superconductivity. Indeed, experimental and theoretical studies have long proposed that the PG is a signature of precursor pairing[9, 10]. Other models incorporating non-local

interactions, such as cluster dynamical mean-field theory[11] or the dual fermion approach[12], attribute both PG formation and electron pairing to the presence of short-range spin correlations that persist beyond the doping level at which antiferromagnetic (AFM) order is destroyed. Recent measurements of the Hall effect[13, 14] and specific heat[15] found evidence for an abrupt change in the carrier density (n) and electronic specific heat coefficient (γ) near p^*, prompting suggestions that the PG may terminate at a quantum critical point. Although other transport and thermodynamic properties are yet to be captured within such a scenario[16], this prospect has nonetheless motivated the discovery of a multiplicity of competing orders within the PG regime and, more broadly, the search for related phenomena in layered materials that exhibit similar attributes to the cuprates. In this regard, the single-layer iridate Sr_2IrO_4 has proven to be an excellent case study.

Sr_2IrO_4 is isostructural to the archetypal cuprate La_2CuO_4 (albeit with a distorted array of IrO_6 octahedra) and features a single half-filled electronic band with **AQ8** $J_{eff} = 1/2$ relevant for its low-energy excitations[17]. The undoped compound is an AFM Mott insulator due to the strong spin–orbit coupling of Ir 5*d* orbitals, which cooperates with the moderate Coulomb interaction to realize a Mott state. Upon ~4% electron doping, the antiferromagnetism is destroyed[18] although short-range spin correlations persist to much higher doping concentrations[19, 20, 21, 22]. Surface-sensitive probes have revealed a PG state with striking similarities to that found in the cuprates, including a suppression of spectral weight around the zone edges and a *d*-wave energy gap by angle-resolved photoemission spectroscopy (ARPES)[23, 24, 25] and a V-shaped PG coexisting with a U-shaped Mott gap by scanning tunnelling microscopy[26]. As a result, Sr_2IrO_4 has been considered as a close 5*d* analogue of the high-T_c cuprates. Several theoretical studies[27, 28, 29] have predicted unconventional superconductivity under sufficient electron doping. As of now, however, superconductivity has not been confirmed. Moreover, a systematic investigation of the transport and thermodynamic characteristics of electron-doped Sr_2IrO_4, which is essential for understanding the nature of PG in this 5*d* Mott insulator, has been lacking.

Here we report transport and specific heat measurements on a series of $Sr_{2-x}La_xIrO_4$ single crystals covering a wide range of La doping ($0 \le x \le 0.20$). The evolution of the electronic ground state with carrier doping reveals striking parallels in the iridates and cuprates, which allowed us to identify the critical doping level at which the PG closes in $Sr_{2-x}La_xIrO_4$. The absence of superconductivity in the iridates not only enables its electronic ground state to be studied down to low temperatures and magnetic field strengths, but also emphasizes the disparate nature of the PG and superconducting ground states.

Electrical transport

Figure 1 shows the Hall resistivity ρ_{yx} measured for an extensive series of $Sr_{2-x}La_xIrO_4$ crystals. The substitution of Sr^{2+} by La^{3+} introduces one additional electron per unit formula. As such, the La content x corresponds to the nominal electron doping on the Ir^{4+} ion. We found that ρ_{yx} was negative and varied linearly with the magnetic field (H), even in field strengths up to 35 T (Supplementary Fig. 1), consistent with the expectation that the doped electrons are solely responsible for the charge transport in $Sr_{2-x}La_xIrO_4$. For a material with a single type of charge carrier and an electron mean-free-path ℓ that is isotropic in k-space, the magnitude of the Hall coefficient R_H is set by the Hall carrier density n_H: **AQ9** **AQ10**

$$R_H = \frac{\rho_{yx}}{\mu_0 H} = \frac{1}{n_H e}, \quad (1)$$

and is independent of the magnitude of ℓ, that is the level of disorder. Here, e is the elementary charge. At a fixed low temperature $T = 30$ K, $|\rho_{yx}|$ and $|R_H|$ decreased by more than two orders of magnitude as x was increased from $x = 0$ to $x \approx 0.20$ (Fig. 1a–c). Given the lack of any nonlinearity in $\rho_{yx}(H)$ that might indicate the presence of two carrier types (electrons and holes), this marked decrease in $|R_H|$ most naturally reflects a substantial increase in the number of itinerant carriers upon electron doping. In addition, we observed a qualitative change in the temperature dependence of $R_H(T)$ as x was increased beyond a threshold value $x_c \approx 0.16$. For $x < 0.14$, $|R_H(T)|$ increased monotonically as T decreased, presumably due to an energy gap at the Fermi level E_F and a loss of itinerant carriers as thermal fluctuations were reduced. In contrast, for $x > 0.17$, $|R_H|(T)$ exhibited a maximum at $T \approx 50$ K, below which a modest reduction in $|R_H|$ occurred. The marked increase in n_H, coupled with the emergence of a non-monotonic form for $R_H(T)$, suggests that there was a recovery of the spectral weight at E_F and a marked change in the electronic ground state in $Sr_{2-x}La_xIrO_4$ beyond $x = x_c$. Moreover, we found a sharp increase in the longitudinal conductivity σ_{xx} at low T as $x \to 0.14$ (Fig. 2), reaching a plateau that corresponded to the conductance quantum per IrO_2 plane, $\frac{h}{e^2}\frac{1}{d}$. The subsequent dip in carrier mobility μ_H as x was increased beyond 0.17 probably reflects the enhanced scattering as more carriers became delocalized. Intriguingly, as later shown in Fig. 4, the effective zero-temperature carrier density per unit cell volume $|n_H|V_{uc}(0)$ closely tracked $n = x$ up to $x \approx 0.13$, above which $|n_H|V_{uc}$ crossed over to approaching $n = 1 + x$ at $x \approx 0.20$, the maximum La content that can presently be achieved in bulk crystals. Note that this marked crossover in n_H is robust and does not depend on the extrapolation method used (Supplementary Fig. 2). This $n = x$ to $n = 1 + x$ evolution of the effective carrier density in electron-doped Sr_2IrO_4 across $x_c = 0.16$ is our first key experimental finding.

Fig. 1

Hall effect in $Sr_{2-x}La_xIrO_4$.

a–**c**, Magnetic-field-dependent Hall resistivity $\rho_{yx}(H)$ measured at specified temperatures for $x = 0$ (**a**), $x = 0.122$ (**b**) and $x = 0.196$ (**c**). A negative ρ_{yx} that varies linearly with the applied magnetic field was found for all x and T. Note that $|\rho_{yx}|$ decreases by orders of magnitude as x increases, reflecting the large increase in the effective Hall carrier density $|n_H|$ induced by La doping. The high noise level for $x = 0$ at low T is caused by noise in the longitudinal component of the measured signals in the highly insulating state. **d**, Absolute Hall coefficient $|R_H|$ as a function of La doping x and temperature T plotted on a log-linear scale. Dashed lines are linear extrapolations of the $R_H(T)$ data to the zero-temperature axis. The semi-filled triangle marks the corresponding R_H for an isotropic, fully delocalized $J_{eff} = 1/2$ band at half **AQ11** filling.

Source data

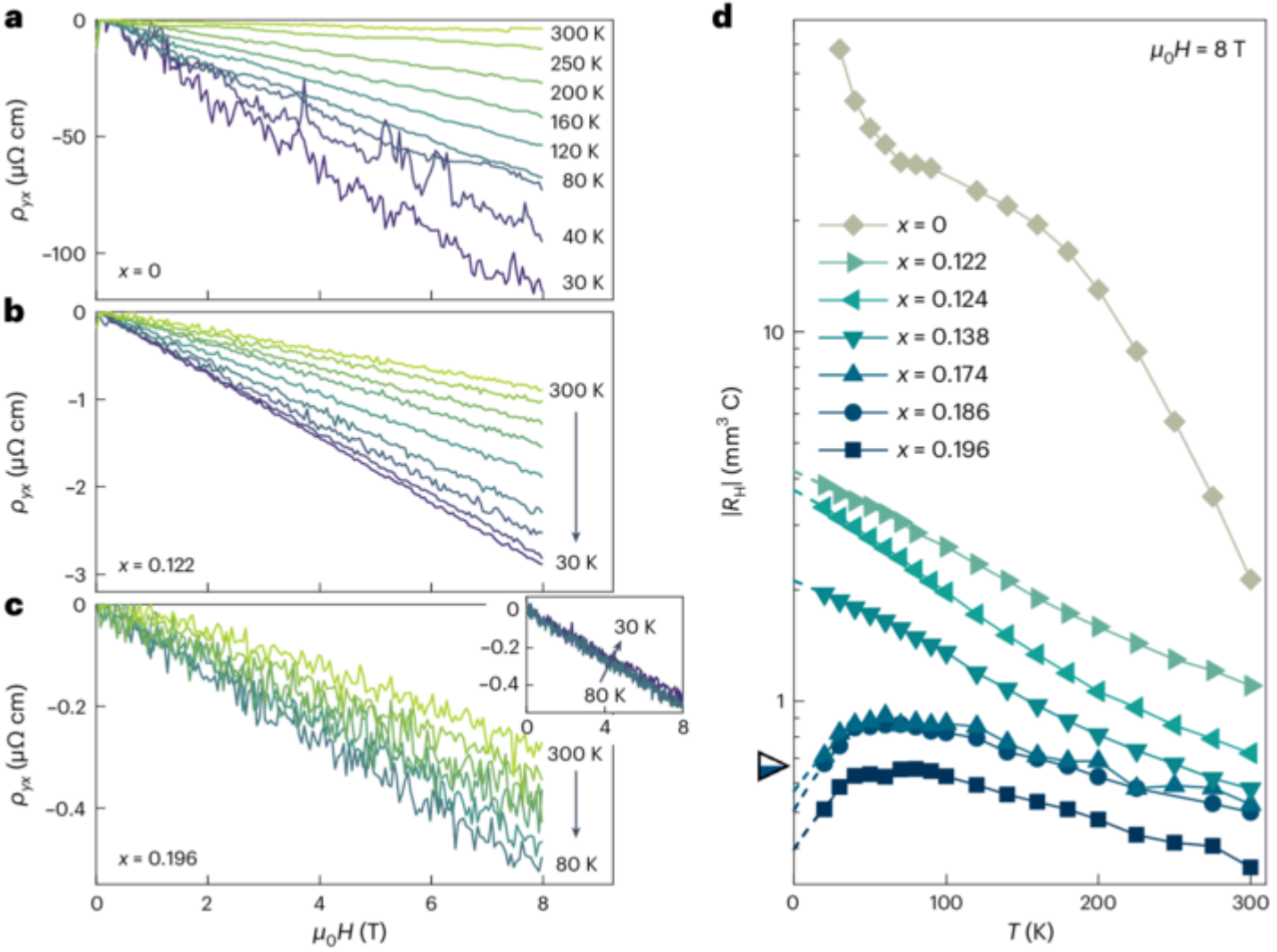

Fig. 2

Longitudinal resistivity and mobility of $Sr_{2-x}La_xIrO_4$.

a, $\rho_{xx}(T)$ for representative x showing a rapid suppression of low-T ρ_{xx} with electron doping. For $x = 0.035$ and 0.10, ρ_{xx} data were unavailable due to the small size of the sample (<400 μm). Dashed lines are fits to the data below 50 K using a variable range hopping model in three dimensions: $\rho = \rho_0 \exp (T_0/T)^{1/4}$. **b**, Carrier mobility calculated using $\mu_H = R_H/\rho_{xx}$ for the same samples shown in **a**. The grey shaded region is the temperature range in which R_H is not available. **AQ12** Open symbols at $T = 0$ were calculated using the extrapolated $R_H(T = 0)$ and fitted ρ_{xx} at 2 K. **AQ13** **c**, Conductivity σ_{xx} at 2 K for all x studied. The horizontal dashed line corresponds to the conductance quantum per IrO_2 plane, $\frac{h}{e^2}\frac{1}{d}$. **d**, μ_H in the $T = 0$ limit. Both σ_{xx}(2 K) and $\mu_H(0)$ show a rapid initial increase as $x \to 0.14$, above which a moderate variation is induced by increasing x. Each data point reflects measurements on a single crystal. Error bars in x reflect the standard uncertainty in La content from energy-dispersive X-ray (EDX) measurements and error bars in n_H reflect the geometric uncertainty for a given sample.

Source data

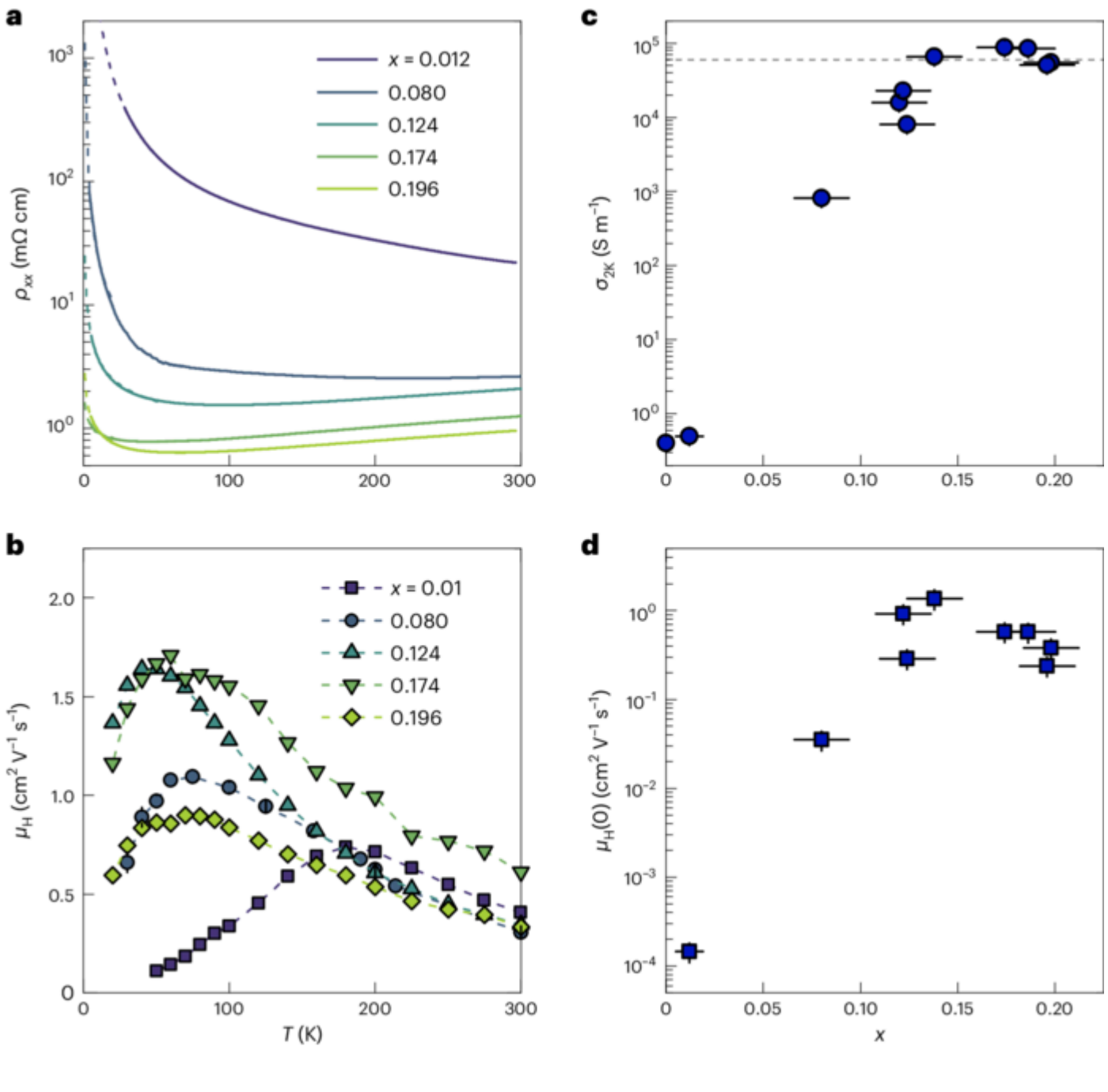

Specific heat

Measurements of the specific heat at low T allow us to directly probe the electronic density of states at E_F and track its evolution as a function of x. Figure 3 shows the specific heat C of $Sr_{2-x}La_xIrO_4$ below 20 K, plotted as C/T versus T^2, measured on small flakes of the same crystals used for the Hall measurements. Between 10 and 20 K ($100\ K^2 \leq T^2 \leq 400\ K^2$), C/T varied approximately linearly with T^2 with a slope $\beta \approx 0.43$ mJ mol^{-1} K^{-2}, consistent with previous reports for polycrystalline Sr_2IrO_4 (refs. [30, 31]) and corresponding to a Debye temperature $\Theta_D \approx 320$ K. To quantitatively extract the electronic specific heat, we fitted the C/T data between 2 and 5 K (the lowest T window in which an approximately linear-in-T^2 behaviour was observed) using:

$$\frac{C}{T} = \gamma + \beta T^2, \quad (2)$$

where γ and β correspond to the electronic and phononic contributions, respectively. For very lightly doped $Sr_{2-x}La_xIrO_4$ with $x = 0.012$ or 0.036, a small $\gamma = 0.65$–1.4 mJ mol^{-1} K^{-2} was found (Fig. 3b), comparable to that observed in pristine Sr_2IrO_4 ($\gamma = 1.5 \pm 0.5$ mJ mol^{-1} K^{-2}; refs. [30, 31]). As x was increased, γ showed a substantial enhancement followed by a sharp drop at $x \approx 0.20$. The largest γ was found for $x = 0.138$ being $\gamma = 9.5 \pm 1.4$ mJ mol^{-1} K^{-2}, approximately one order of magnitude larger than that found for the low-doped material. Note that the nuclear contribution was negligibly small above 1 K (Supplementary Fig. 3). Also note a similar enhancement in the measured C/T at $T = 2$ and 1 K (Supplementary Fig. 4), for which the phononic contribution is expected to decrease very sharply, implying that our estimate for the doping dependence of γ is robust in the $T = 0$ limit. This large enhancement of low-T specific heat centred around $x_c = 0.16$, which coincides with the marked increase in carrier density as summarized in Fig. 4, is our second key finding.

Fig. 3

Low-temperature specific heat of $Sr_{2-x}La_xIrO_4$.

a, Specific heat measured in zero applied magnetic field, plotted as C/T versus T^2, between 1.5 and 20 K. A smooth, monotonic, addenda background was subtracted from the data shown. The slopes $d(C/T)/d(T^2)$ between 10 and 20 K are similar for all x, indicating that the phonon contribution varied little with La doping. **b**, Low-temperature region ($T \leq 5$ K) for the data shown in **a** with a vertical shift of 10 mJ mol^{-1} K^{-2} applied to each x for clarity. Grey dashed lines are fits made to the data between 2 and 5 K using $C/T = \gamma + \beta T^2$, and the vertical shadings correspond to the magnitude of zero-temperature intercepts $\gamma = C/T(T = 0)$ for each x. A sizeable enhancement of γ at intermediate La doping $0.122 \leq x \leq 0.174$ was observed.

Source data

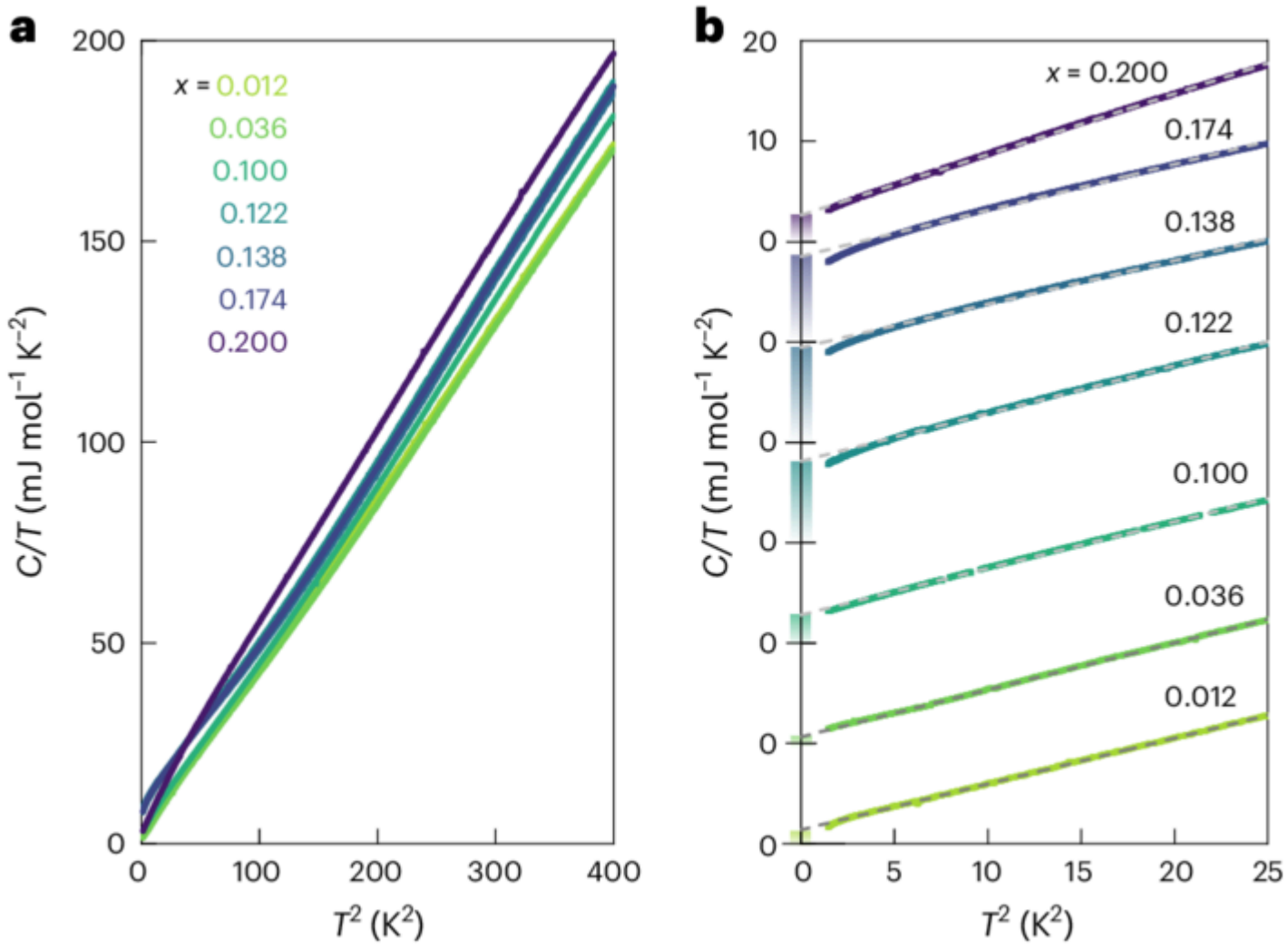

Fig. 4

Doping evolution of the Hall number and specific heat in the T = 0 limit.

a, Absolute Hall number multiplied by the unit cell volume $|n_H|V_{uc}(0)$, which is a measure of the effective carrier number per IrO_2 plane estimated at 0 K, as a function of x. Each data point is an average of the experimental n_H at the lowest measured temperature (20 K for $x > 0.06$ and 30 K for $x < 0.06$) and the extrapolated n_H at 0 K (Fig. 1d). The lower and upper dotted lines correspond to $n = x$ and $n = 1 + x$, respectively. **b**, Electronic specific heat coefficient γ estimated from the extrapolated $C/T(T = 0)$ values. Data at $x = 0$ are reproduced from previous reports[30, 31]. Dashed lines are guides to the eye. A marked enhancement in γ centred around $x = 0.16$ is observed, which coincides with the drastic increase in $|n_H|$. Each data point was measured for a single crystal. Error bars in x reflect the standard uncertainty in La content from EDX measurements. Error bars in n_H reflect the compound uncertainty in sample thickness and 0 K extrapolation (that is, $dn_H(0)/n_H(0) = \sqrt{(dt/t)^2 + (dn_{H0})/dn_{H0})^2}$ where t is the sample thickness and n_{H0} is the fitted 0 K intercept of n_H). AQ14 Error bars in γ reflect the calibration uncertainty of the nanocalorimetry measurements. Three regimes with distinct electronic ground states were identified: a Mott insulator (MI) for $0 \leq x \lesssim 0.085$, a PG state (blue shading) for $0.085 \lesssim x \lesssim 0.17$ and a disordered metal (DM; grey shading) for $x \gtrsim 0.17$.

Source data

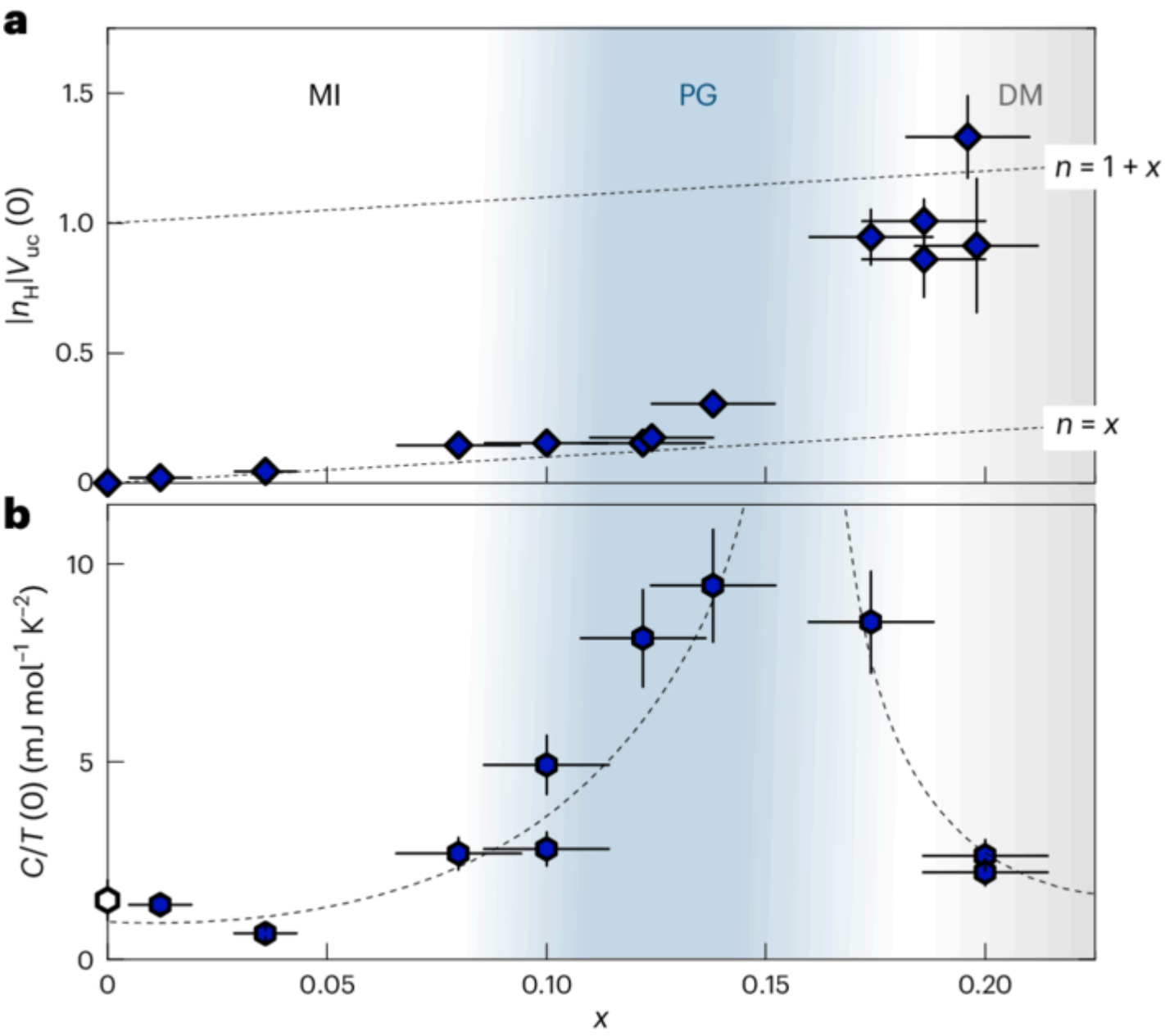

For a quasi-two-dimensional metal, γ is linked to the quasiparticle effective mass m^* (ref. [32]):

$$\gamma = \frac{\pi k_B^2 a^2 N_A}{3\hbar^2 N_{uc}} \sum_i m_i^*, \quad (3)$$

where a is the in-plane lattice parameter, N_A Avogadro's number, N_{uc} the number of formula units in a unit cell and i denotes the distinct Fermi pocket. An enhancement in γ thus indicates a mass enhancement of the itinerant carriers, which can originate from the underlying band structure (for example, on the approach to a van Hove singularity (vHs)) or many-body interactions (for example, critical fluctuations near a quantum critical point). In quantum critical metals, the mass enhancement near a putative quantum critical point typically manifests as a pronounced peak in γ accompanied by a logarithmic divergence at low T (that is, $C/T \propto \ln(1/T)$ as $T \to 0$)[33]. The absence of such a divergent $C/T(T)$ in $Sr_{2-x}La_xIrO_4$ (Supplementary Fig. 3), however, combined with the lack of long-range electronic order near $x = 0.16$ (see below), appears difficult to reconcile with a scenario involving conventional quantum criticality.

Possible origins of the observed crossovers

As $x \to x_c$ from the parent Mott state, we found that the effective zero-temperature carrier density $n_H(0)$ showed a gradual crossover from $n = x$ to $n = 1 + x$, which was accompanied by the conductivity per IrO_2 plane approaching the conductance quantum and a sixfold enhancement in electronic specific heat γ. Beyond x_c, γ dropped markedly in a manner that is reminiscent of what is found in hole-doped $La_{1.6-x}Nd_{0.4}Sr_xCuO_4$ beyond $p^* \approx 0.23$ (ref. [14,15]). Likewise, the evolution of the transport coefficients of $Sr_{2-x}La_xIrO_4$ was qualitatively like that reported for hole-doped cuprates[3,13,14,34,35]. At low doping ($x \lesssim 0.13$), $|n_H|(x) \approx x$, implying that only the doped electrons become mobile, consistent with previous ARPES studies in lightly electron-doped Sr_2IrO_4, which found a small spectral weight at E_F (refs. [25,36]). A similar relation ($n_H(x) \approx p$ determined at $T = 50$ K) has been found for $La_{2-x}Sr_xCuO_4$ (LSCO) below $x = 0.08$ (refs. [3,13]). For $YBa_2Cu_3O_{7-\delta}$ (ref. [13]) and Nd-doped LSCO[14], a sharp crossover from $n_H \approx p$ to $n_H \approx 1 + p$ has been observed in the vicinity of p^*, suggesting that the hole that initially localized in the parent state was recovered as soon as the PG vanished. Such a drastic change in n_H may signify a Fermi surface reconstruction driven by an electronic and structural order parameter with sufficiently long-range correlations. For Nd-LSCO, for example, this is probably spin stripe correlations[37]. For $Sr_{2-x}La_xIrO_4$, the only long-range electronic order known to exist is the (π, π) AFM order, which shares the same reduced Brillouin zone boundary caused by the IrO_6 octahedra rotations. The resultant reconstructed Fermi surface of $Sr_{2-x}La_xIrO_4$ is expected to comprise both electron-like pockets around the ($\pi/2$, $\pi/2$) nodal region and hole-like pockets around the the (0, π) antinodal region[25]. Consequently, the measured Hall signals should include contributions from both Fermi pockets, even if the mobility of both pockets is low. These bipolar contributions would typically give rise to a nonlinearity of $\rho_{yx}(H)$ at sufficiently high H and an $R_H(T = 0)$ value that markedly deviates from expectations for a single conducting channel, neither of which we observed (Supplementary Fig. 1). Moreover, the AFM order is known to vanish at a doping level ($x \leq 0.04$) far below x_c, whereas the lattice distortion does not fundamentally alter the underlying electronic structure (except that it leads to a back-folded shadow band that is photon energy-dependent[23,25,38]). Furthermore, the structural distortion is not suppressed by La doping[21]. Thus, it cannot lead to a profound change in electronic structure across the doping series investigated. It is, therefore, unlikely that Fermi surface reconstruction driven by long-range order can explain the drop in $|n_H|$ below $x_c \approx 0.16$. Indeed, we are not aware of any experimental evidence for an electronic or structural transition induced by La doping in $Sr_{2-x}La_xIrO_4$ (Supplementary Information Section 6.2).

Models of Fermi surface reconstruction in the absence of long-range order within the PG regime have been proposed for the cuprates[39, 40, 41]. Numerical calculations[42, 43] based on the model proposed by Yang, Rice, and Zhang[39] show that both n_H and γ can exhibit a marked enhancement near p^* due to the appearance of the reconstructed electron pocket. Although it has not yet been established whether Yang, Rice, and Zhang's model is applicable to Sr_2IrO_4, evidence for the persistence of short-range AFM fluctuations up to 20% electron doping has been reported[20]. A recent dynamical mean-field study of Sr_2IrO_4 (ref. [44]) found that the electronic ground state evolves with electron doping through several distinct regimes: a Mott-insulating state at low dopings, a PG and a differentiated regime with suppressed spectral weight near the zone boundary at intermediate dopings and a uniform metallic regime in which the electronic states at E_F become increasingly more coherent with increasing doping. Such a scenario is consistent with the $n \approx x$ to $n \approx 1 + x$ crossover, though it is not yet clear how γ and m^* would evolve within such a model.

The PG in cuprates has also been interpreted as a spatially inhomogeneous, doping-dependent, localization gap Δ that at low doping localizes exactly one hole per CuO_2 unit[45]. In this picture, the $n_H \approx p$ to $n_H \approx 1 + p$ crossover is a gradual one, as observed in certain cuprate families[35], due to its broad distribution in energy and real-space heterogeneity. The holes originally localized in the parent Mott state become fully delocalized only at the edge of the superconducting dome where the PG is assumed to close. Although this picture can account for a gradual crossover in n_H with doping, the link between the crossover and PG closing is not yet proven[35, 46].

An alternative driver for the enhanced γ in $Sr_{2-x}La_xIrO_4$ is a vHs crossing at which the quasi-two-dimensional Fermi surface undergoes a Lifshitz transition from electron-like to hole-like. In such a scenario, n_H (in the isotropic-ℓ limit) is expected to change sign. Were ℓ to be anisotropic, however, n_H may no longer correspond to the carrier concentration or its character[47, 48] (Methods). In analogy with the cuprates, the observation of Fermi arcs in the PG regime suggests a 'nodal–antinodal dichotomy' that manifests itself at higher doping with k-dependent scattering and a departure from the isotropic-ℓ limit. In this circumstance, one would expect the regions with hole-like curvature near the antinodes to have a shorter ℓ than the electron-like sections close to the nodes. Consequently, the Hall conductivity σ_{xy} would continue to be dominated by those regions of the Fermi surface with electron-like curvature and R_H would remain negative. The hole-like regions would, nevertheless, contribute progressively to the total conductivity σ_{xy} and σ_{xx}, resulting in a reduction in $|R_H|$ and a corresponding growth in $|n_H|$. Thus, the enhancements of $|n_H|$, σ_{xx} and γ may be consistent with a scenario based on a vHs crossing near $x_c \approx 0.16$.

Although the coincidence of the vHs crossing and PG closure appears to be well established for LSCO[49], that is not the case for $Sr_{2-x}La_xIrO_4$. Previous band structure calculations found that the vHs in Sr_2IrO_4 lies at approximately 0.12 eV above the chemical potential (irrespective of the inclusion of lattice distortions), corresponding to electron doping exceeding 20%[28, 50, 51]. This conclusion is confirmed by our tight-binding calculations, which locate the vHs at $x \approx 0.29$ (Supplementary Figs. 5 and 6). All these calculations appear to place the vHs crossing in $Sr_{2-x}La_xIrO_4$ well beyond x_c, although future ARPES experiments on more highly doped crystals should help to confirm its location and clarify its impact on the thermodynamic properties. Irrespective of the vHs location, without PG closure and a contribution from the hole-like regions to σ_{xy}, the measured n_H would not approach $n = 1 + x$. Moreover, the n_H crossover to $n = x$ would not occur without a PG opening, as the ℓ-anisotropy required to reproduce the crossover is unphysically large (Supplementary Table 1). Hence, we can conclude that the drop in n_H from $n = 1 + x$ below x_c is associated with a loss of itinerant carriers upon the PG opening. This observation not only identifies the location of PG closure, it also places $Sr_{2-x}La_xIrO_4$ alongside the cuprates in the second category of doped Mott insulators with the electronic specific heat coefficient diminishing upon approaching the Mott state, and it implies that non-local interactions must play a prominent role in the physics of the iridates.

Despite the striking similarities in the normal-state properties of $Sr_{2-x}La_xIrO_4$ and the cuprates, to date no robust signatures of superconductivity have been reported for the former. In this regard, it is instructive to compare the characteristic energy scales of Sr_2IrO_4 to those of isostructural La_2CuO_4. We summarize in Supplementary Table 2 the leading terms associated with carrier hopping (t), spin correlations (J) and charge correlations (U) of the two compounds. (Note that for Sr_2IrO_4, J characterizes the Hund's coupling, which promotes spin exchange[52]). As the 5d orbitals are more spatially extended, t is larger for Sr_2IrO_4 whereas J and U are smaller. It has been pointed out previously[52] that the phase space available for stable superconductivity reduces with increasing J/U whereas it expands with increasing U/t, with a suggested critical value of $U/t > 6$ for the realization of superconductivity. Though J/U is similarly small in both oxides, U/t is substantially reduced for Sr_2IrO_4 and very close to (or slightly below) the critical value. It is possible that a distinctly favourable energy landscape for superconductivity is realized only for the cuprates, which marks the key difference between the two oxide families, despite them sharing the same PG phenomenology. A more mundane reason for the absence of superconductivity is the higher level of disorder reflected in the low-T resistivity upturns (at sufficiently high dopings). In underdoped LSCO (x = 0.06), the in-plane resistivity has a minimum[3] with $\rho_{ab} \approx 600$ μΩ cm at 50 K. By contrast, for $Sr_{2-x}La_xIrO_4$ ($x \approx 0.17$, a significantly higher carrier density), $\rho_{ab} \approx 650$ μΩ cm at 50 K, implying a lower overall carrier mobility. **AQ15** The growth of cleaner iridates, were it ever to be possible, would obviously help to address this point. Moreover, the PG is seen to be robust to the presence of disorder.

In summary, our transport and thermodynamic measurements on a series of $Sr_{2-x}La_xIrO_4$ crystals revealed two defining bulk signatures regarding the fate of carriers doped into a 5d Mott insulator Sr_2IrO_4: the density of the itinerant carriers undergoes a dramatic reduction upon the removal of electron dopants at $x_c \approx 0.16$ whereas the electronic specific heat coefficient is strongly enhanced upon approaching x_c. Our findings indicate that the low-T electronic ground state of $Sr_{2-x}La_xIrO_4$ undergoes a profound transformation with electron doping, and aided by numerical calculations, we conclude that: (1) The loss of itinerant carriers signifies the PG opening near x_c. (2) The concomitant enhancement in quasiparticle effective mass is not associated with an identifiable long-range order parameter or a quantum critical point. (3) A bulk pseudogapped state does not promote superconductivity in a doped 5d Mott insulator. The striking similarity between the PG phenomenology of hole-doped cuprates and electron-doped Sr_2IrO_4 thus suggests that PG formation is generic to doped quasi-two-dimensional AFM Mott insulators but is not itself a precursor to superconductivity.

Methods

Single-crystal growth

Crystals of $Sr_{2-x}La_xIrO_4$ were grown using a flux method with an off-stoichiometric mixture of $SrCO_3$:IrO_2:La_2O_3 and anhydrous $SrCl_2$ flux in a small Pt crucible (30 ml) with a loose lid. For $x < 0.1$, starting materials with a typical ratio of $SrCO_3$:IrO_2:La_2O_3:$SrCl_2$ = $1.9 - 2x : 1.0 : x/2 : 9.0$ were heated to 1,245 °C, held for 12 h, cooled to 1,100 °C at a rate ~8 °C h^{-1} then quenched to room temperature. For $x > 0.1$, starting materials with a typical ratio of $SrCO_3$:IrO_2:La_2O_3:$SrCl_2$ = 1.5: 1.0: 18: 9.0 were heated to 1,350 °C and held for 30 h then quenched. The resulting square platelet

crystals had a typical lateral size of 0.2–2.0 mm and were separated from the flux by rinsing with deionized water. The La content x, which corresponds to the nominal electron doping on the Ir site, was determined for each measured crystal using energy-dispersive X-ray (EDX) spectroscopy on cleaved surfaces using a scanning electron microscope (JSM-6610LV, JEOL) and an energy-dispersive X-ray spectroscope (Oxford Instruments), with a typical uncertainty in x of 0.01–0.02. AQ16 Note that the reproducibility between growth runs was poor, with identical starting constituents producing different results. A 50% variation in EDX-measured x values was often found across each batch compared to the nominal x.

Magnetotransport measurements

Platelets of $Sr_{2-x}La_xIrO_4$ with typical dimensions of (600 × 250 × 75) μm^3 were selected for electrical transport measurements. Gold wires of 25 or 50 μm diameter were attached to the crystals using silver paint (DuPont 6838), with the crystal sides carefully painted to eliminate the c-axis contribution, and annealed in flowing oxygen at 450 °C for 10 min to achieve sub-ohm contact resistances. Measurements in magnetic fields up to 8 T, applied along the c-axis, were performed using a cryogen-free measurement system (Cryogenic Ltd). Measurements up to 35 T were performed using a Florida–Bitter magnet coupled to a ^{4}He-flow cryostat at the High Field Magnet Laboratory at Radboud University. Longitudinal resistivity measurements were performed down to ~3 K (except for $x = 0.012$, which were down to 20 K) and Hall measurements down to 20 K. Note that small temperature fluctuations at $T < 20$ K, where all samples showed a resistive upturn with a sizeable $|d\rho_{xx}/dT|$ (Fig. 2), led to increased noise levels in the measured Hall signals (due to imperfect contact alignment) and prevented a reliable extraction of the Hall resistivity below 20 K. The noise in our ρ_{yx} measurements was at a constant level of ~0.02 μΩ cm for $x > 0.10$. For $x \leq 0.10$, the noise level was highly dependent on x and T due to the divergent longitudinal component, reaching 2 μΩ cm at 30 K for $x = 0$. Nonetheless, the percentage uncertainty in R_H at 8 T was less than 5% for all x and T, and is accounted for by the error bars of the corresponding $n_H(0)$.

Specific heat measurements

The present series of $Sr_{2-x}La_xIrO_4$ crystals had a low mass (submicrogram), which limited the feasibility of standard specific heat methods. To perform measurements on miniature crystals, we adopted a Si-N membrane-based nanocalorimetry method, which has been successfully employed on materials with submicrogram masses[53]. Samples from the same crystals used for the transport measurements were cleaved to yield flakes with clean surfaces with lateral dimensions of 50–100 μm and thicknesses of 10–30 μm. Measurements were performed in a dilution refrigerator (Bluefors) with a differential calorimeter operating using the a.c. steady-state method, with automatic adjustments of thermometer bias, a.c. heating and temperature oscillation frequency. Samples were mounted with a very small amount of grease (Apiezon N), measured separately before sample mounting. The $NiCrSiO_x$ thin-film cermet calorimeter thermometers[54] were operated at the nth harmonic (n between 3 and 8) of the a.c. heater to provide a temperature oscillation response at the $n + 2$ harmonic. Absolute temperature control was obtained through a local offset heater on the calorimeter membrane, with the dilution refrigerator sitting at base temperature. The reference cell thermometer was used only as a thermometer bridge to provide a clean, high-resolution, differential measurement of the temperature oscillation.

Numerical calculations

We adopted the tight-binding model developed in ref. [28] to parameterize the Fermi surface of Sr_2IrO_4. The doping of electrons was modelled by shifting the chemical potential to match the enclosed Fermi surface area with the expected value (that is, the corresponding Luttinger count). We found that the vHs lies at $n \approx 1.29$ (29% electron doping), consistent with a previous report, which found that the vHs occurred above 20% electron doping[50]. For the electronic specific heat γ, we used the electronic density of states D derived from the tight-binding Fermi surface parametrization:

$$\gamma = \frac{\pi^2}{3} k_B^2 D, \tag{4}$$

$$D = \frac{1}{2\pi^2 d} \int_0^{2\pi} \frac{\mathbf{k}_F}{\hbar \mathbf{v}_F} \, d\theta, \tag{5}$$

where $\mathbf{k}_F$ ($\mathbf{v}_F$) is the Fermi wavevector (velocity), d the distance between two IrO_2 planes and θ the azimuthal angle around the two-dimensional Fermi surface. For longitudinal and Hall resistivities, we used the Boltzmann transport equations generalized to a two-dimensional system with anisotropic scattering:

$$\sigma_{ij} = \frac{e^2}{2\pi^2 \hbar d} \int_0^{2\pi} \tau \frac{\mathbf{v_i} \cdot \mathbf{v_j}}{|v_F| \cos \phi} k_F \, d\theta, \tag{6}$$

where ϕ is the angle between v_F and k_F.

Online content

Any methods, additional references, Nature Portfolio reporting summaries, source data, extended data, supplementary information, acknowledgements, peer review information; details of author contributions and competing interests; and statements of data and code availability are available at https://doi.org/10.1038/s41567-024-02564-3.

Supplementary information

The online version contains supplementary material available at https://doi.org/10.1038/s41567-024-02564-3.

Acknowledgements

We thank F. Baumberger, A. Georges and A. Tamai for fruitful discussions. We would like to thank R. D. H. Hinlopen for assistance with the numerical calculations and G. Stenning and D. Nye for help with the PPMS and Smartlab instruments in the Materials Characterisation Laboratory at the ISIS Neutron and Muon Source. AQ17 We acknowledge the support of the High Field Magnet Laboratory (Grant No. HFML-RU/NWO-I), a member of the European Magnetic Field Laboratory. This work was supported by the European Research Council under the European Union's Horizon 2020 research

and innovation programme (Grant Agreement No. 835279-Catch-22), by the Swedish Research Council (Grant No. 2021-04360) and by the UK Engineering and Physical Sciences Research Council (Grant Nos. EP/N034694/1 and EP/V02986X/1).

Author contributions

Y.T.H. designed the project. R.S.P. and A.T. grew and characterized the crystals. Y.T.H., M.B. and C.D. performed the magnetotransport measurements. A.R. performed the specific heat measurements. Y.T.H. performed the numerical calculations. Y.T.H. and N.E.H. wrote the manuscript with inputs from all authors.

Peer review

Peer review information

Nature Physics thanks Danfeng Li and the other, anonymous, reviewer(s) for their contribution to the peer review of this work.

Data availability

Source data are provided with this paper. Any additional data are available from the corresponding authors upon request.

Code availability

The codes associated with the band structure and transport coefficient calculations that support this study are available from the corresponding authors upon request.

Competing interests

The authors declare no competing AQ18 interests.

Supplementary information

Supplementary Information

Supplementary Figs. 1–6, discussion and Tables 1 and 2.

Source data

Source Data Fig. 1

Measured experimental data.

Source Data Fig. 2

Measured experimental data and calculated transport coefficients.

Source Data Fig. 3

Measured experimental data.

Source Data Fig. 4

Calculated transport and thermodynamic coefficients.

References

1. Imada, M. Two types of Mott transitions. *J. Phys. Soc. Jpn* **62**, 1105–1108 (1993).

2. Tokura, Y. et al. Filling dependence of electronic properties on the verge of metal–Mott-insulator transition in $Sr_{1-x}La_xTiO_3$. *Phys. Rev. Lett.* **70**, 2126–2129 (1993).

3. Ando, Y., Kurita, Y., Komiya, S., Ono, S. & Segawa, K. Evolution of the Hall coefficient and the peculiar electronic structure of the cuprate superconductors. *Phys. Rev. Lett.* **92**, 197001 (2004).

4. Padilla, W. J. et al. Constant effective mass across the phase diagram of high-T_c cuprates. *Phys. Rev. B* **72**, 060511 (2005).

5. Norman, M. R. et al. Destruction of the Fermi surface in underdoped high-T_c superconductors. *Nature* **392**, 157–160 (1998).

6. Alloul, H., Ohno, T. & Mendels, P. ^{89}Y NMR evidence for a Fermi-liquid behavior in $YBa_2Cu_3O_{6+x}$. *Phys. Rev. Lett.* **63**, 1700–1703 (1989).

7. Keimer, B., Kivelson, S. A., Norman, M. R., Uchida, S. & Zaanen, J. From quantum matter to high-temperature superconductivity in copper oxides. *Nature* **518**, 179–186 (2015).

8. Tallon, J. L., Storey, J., Cooper, J. R. & Loram, J. W. Locating the pseudogap closing point in cuprate superconductors: absence of entrant or reentrant behavior. *Phys. Rev. B* **101**, 174512 (2018).

9. Emery, V. J. & Kivelson, S. A. Importance of phase fluctuations in superconductors with small superfluid density. *Nature* **374**, 434–437 (1995).

10. Zhou, P. et al. Electron pairing in the pseudogap state revealed by shot noise in copper oxide junctions. *Nature* **572**, 493 (2019).

11. Park, H., Haule, K. & Kotliar, G. Cluster dynamical mean field theory of the Mott transition. *Phys. Rev. Lett.* **101**, 186403 (2008).

12. Rubtsov, A. N., Katsnelson, M. I. & Lichtenstein, A. I. Dual fermion approach to nonlocal correlations in the Hubbard model. *Phys. Rev. B* **77**, 033101 (2008).

13. Badoux, S. et al. Change of carrier density at the pseudogap critical point of a cuprate superconductor. *Nature* **531**, 210–214 (2016).

14. Collignon, C. et al. Fermi-surface transformation across the pseudogap critical point of the cuprate superconductor $La_{1.6-x}Nd_{0.4}Sr_xCuO_4$. *Phys. Rev. B* **95**, 224517 (2017).

15. Michon, B. et al. Thermodynamic signatures of quantum criticality in cuprate superconductors. *Nature* **567**, 218–222 (2019).

16. Hussey, N. E., Buhot, J. & Licciardello, S. A tale of two metals: contrasting criticalities in the pnictides and hole-doped cuprates. *Rep. Prog. Phys.* **81**, 052501 (2018).

17. Bertinshaw, J., Kim, Y. K., Khaliullin, G. & Kim, B. J. Square lattice iridates. *Annu. Rev. Condens. Matter Phys.* **10**, 315–336 (2019).

18. Chen, X. et al. Influence of electron doping on the ground state of $(Sr_{1-x}La_x)_2IrO_4$. *Phys. Rev. B* **92**, 075215 (2015).

19. Gretarsson, H. et al. Persistent paramagnons deep in the metallic phase of $Sr_{2-x}La_xIrO_4$. *Phys. Rev. Lett.* **117**, 107001 (2016).

20. Pincini, D. et al. Anisotropic exchange and spin-wave damping in pure and electron-doped Sr_2IrO_4. *Phys. Rev. B* **96**, 075162 (2017).

21. Horigane, K. et al. Magnetic phase diagram of $Sr_{2-x}La_xIrO_4$ synthesized by mechanical alloying. *Phys. Rev. B* **7**, 064425 (2018).

22. Rodan, S. T. et al. Quantum critical nature of the short-range magnetic order in $Sr_{2-x}La_xIrO_4$. *Phys. Rev. B* **98**, 214412 (2018).

23. Kim, Y. K. et al. Fermi arcs in a doped pseudospin-1/2 Heisenberg antiferromagnet. *Science* **345**, 187–190 (2014).

24. Kim, Y. K., Sung, N. H., Denlinger, J. D. & Kim, B. J. Observation of a *d*-wave gap in electron-doped Sr_2IrO_4. *Nat. Phys.* **12**, 37–41 (2015).

25. de la Torre, A. et al. Collapse of the Mott gap and emergence of a nodal liquid in lightly doped Sr_2IrO_4. *Phys. Rev. Lett.* **115**, 176402 (2015).

26. Battisti, I. et al. Universality of pseudogap and emergent order in lightly doped Mott insulators. *Nat. Phys.* **13**, 21–25 (2017).

27. Wang, F. & Senthil, T. Twisted Hubbard model for Sr_2IrO_4: magnetism and possible high-temperature superconductivity. *Phys. Rev. Lett.* **106**, 136402 (2011).

28. Watanabe, H., Shirakawa, T. & Yunoki, S. Monte Carlo study of an unconventional superconducting phase in iridate oxide $J_{\mathrm{eff}} = 1/2$ Mott insulators induced by carrier doping. *Phys. Rev. Lett.* **110**, 027002 (2013).

29. Meng, Z. Y., Kim, Y. B. & Kee, H.-Y. Odd-parity triplet superconducting phase in multiorbital materials with a strong spin–orbit coupling: application to doped Sr_2IrO_4. *Phys. Rev. Lett.* **113**, 177003 (2014).

30. Carter, S. A. et al. Mechanism for the metal–insulator transition in $Sr_2Ir_{1-x}Ru_xO_4$. *Phys. Rev. B* **51**, 17184 (1995).

31. Kini, N. S., Strydom, A. M., Jeevan, H. S., Geibel, C. & Ramakrishnan, S. Transport and thermal properties of weakly ferromagnetic Sr_2IrO_4. *J. Phys.: Condens. Matter* **18**, 8205–8216 (2006).

32. Mackenzie, A. P. et al. Calculation of thermodynamic and transport properties of Sr_2RuO_4 at low temperatures using known Fermi surface parameters. *Phys. C.: Supercond.* **263**, 510–515 (1996).

33. Löhneysen, H., Rosch, A., Vojta, M. & Woelfle, P. Fermi-liquid instabilities at magnetic quantum phase transitions. *Rev. Mod. Phys.* **79**, 1015 (2007).

34. Laliberté, F. et al. Origin of the metal-to-insulator crossover in cuprate superconductors. Preprint at https://arxiv.org/abs/1606.04491 (2016). AQ19

35. Putzke, C. et al. Reduced Hall carrier density in the overdoped strange metal regime of cuprate superconductor. *Nat. Phys.* **17**, 826–831 (2021).

36. Brouet, V. et al. Transfer of spectral weight across the gap of Sr_2IrO_4 induced by La doping. *Phys. Rev. B* **92**, 081117(R) (2015).

37. Ma, Q. et al. Magnetic field tuning of parallel spin stripe order and fluctuations near the pseudogap quantum critical point in $La_{1.36}Nd_{0.4}Sr_{0.24}CuO_4$. *Phys. Rev. B* **106**, 214427 (2022).

38. Peng, S. et al. Electronic nature of the pseudogap in electron-doped Sr_2IrO_4. *npj Quantum Mater.* **7**, 58 (2022).

39. Yang, K.-Y., Rice, T. M. & Zhang, F.-C. Phenomenological theory of the pseudogap state. *Phys. Rev. B* **73**, 174501 (2006).

40. Chatterjee, S. & Sachdev, S. Fractionalized Fermi liquid with bosonic chargons as a candidate for the pseudogap metal. *Phys. Rev. B* **94**, 205117 (2016).

41. Morice, C., Montiel, X. & Pepin, C. Evolution of Hall resistivity and spectral function with doping in the SU(2) theory of cuprates. *Phys. Rev. B* **96**, 134511 (2017).

42. Storey, J. G. Hall effect and Fermi surface reconstruction via electron pockets in the high-T_c cuprates. *Europhys. Lett.* **113**, 27003 (2016).

43. Verret, S., Simard, O., Charlebois, M., Senechal, D. & Tremblay, A.-M. S. Phenomenological theories of the low-temperature pseudogap: Hall number, specific heat, and Seebeck coefficient. *Phys. Rev. B* **96**, 125139 (2017).

44. Moutenet, A., Georges, A. & Ferrero, M. Pseudogap and electronic structure of electron-doped Sr_2IrO_4. *Phys. Rev. B* **97**, 115109 (2018).

45. Pelc, D., Popčević, P., Požek, M., Greven, M. & Barišić, N. Unusual behavior of cuprates explained by heterogeneous charge localization. *Sci. Adv.* **5**, eaau4538 (2019).

46. Berben, M. et al. Superconducting dome and pseudogap endpoint in Bi2201. *Phys. Rev. Mater.* **6**, 044804 (2022).

47. Ong, N. P. Geometric interpretation of the weak-field Hall conductivity in two-dimensional metals with arbitrary Fermi surface. *Phys. Rev. B* **43**, 193 (1991).

48. Hussey, N. E. The normal state scattering rate of high-T_c cuprates. *Eur. Phys. J. B* **31**, 495 (2003).

49. Zhong, Y. et al. Differentiated roles of Lifshitz transitions of thermodynamics and superconductivity in $La_{2-x}Sr_xCuO_4$. *Proc. Natl Acad. Sci. USA* **119**, 2204630119 (2022).

50. Yang, Y. et al. Superconductivity in doped Sr_2IrO_4: a functional renormalization group study. *Phys. Rev. B* **89**, 094518 (2014).

51. Lane, C. et al. First-principles calculation of spin and orbital contributions to magnetically ordered moments in Sr_2IrO_4. *Phys. Rev. B* **101**, 155110 (2020).

52. Watanabe, H., Shirakawa, T. & Yunoki, S. Microscopic study of a spin–orbit-induced Mott insulator in Ir oxides. *Phys. Rev. Lett.* **105**, 216410 (2010).

53. Tagliati, S., Krasnov, V. M. & Rydh, A. Differential membrane-based nanocalorimeter for high-resolution measurements of low-temperature specific heat. *Rev. Sci. Instrum.* **83**, 055107 (2012).

54. Fortune, N. A. et al. Wide range thin-film ceramic metal-alloy thermometers with low magnetoresistance. *Phys. Rev. Appl.* **20**, 054016 (2023).